

SPARSE LINEAR OPERATOR IDENTIFICATION WITHOUT SPARSE REGULARIZATION ? APPLICATIONS TO MIXED PIXEL PROBLEM IN TIME-OF-FLIGHT/RANGE IMAGING

Ayush Bhandari, Achuta Kadambi and Ramesh Raskar

Media Laboratory, Massachusetts Institute of Technology, Cambridge, USA.

{ayush, achoo, raskar}@MIT.edu

ABSTRACT

In this paper, we consider the problem of Sparse Linear Operator identification which is also linked with the topic of Sparse Deconvolution. In its abstract form, the problem can be stated as follows: Given a well behaved probing function, is it possible to identify a Sparse Linear Operator from its response to the function? We present a constructive solution to this problem. Furthermore, our approach is devoid of any sparsity inducing penalty term and explores the idea of parametric modeling. Consequently, our algorithm is non-iterative by design and circumvents tuning of any regularization parameter. Our approach is computationally efficient when compared the ℓ_0/ℓ_1 -norm regularized counterparts.

Our work addresses a problem of industrial significance: decomposition of mixed-pixels in Time-of-Flight/Range imaging. In this case, each pixel records range measurements from multiple contributing depths and the goal is to isolate each depth. Practical experiments corroborate our theoretical set-up and establish the efficiency of our approach, that is, speed-up in processing with lesser mean squared error. We also derive Cramér-Rao Bounds for performance characterization.

Index Terms— Deconvolution, sparse linear operator, spectral analysis, system identification and Time-of-Flight (ToF) imaging.

1. INTRODUCTION

1.1. From Sampling Functions to Sensing Operators

Since Shannon's introduction of the topic, sampling theory has been at the heart of signal processing [1]. The field was revitalized by advancements in wavelet/approximation theory, and sampling spaces were extended to a much broader class of finite-energy subspaces: the Shift-Invariant Space [2, 3], its extensions [4, 5] and non-subspace models (cf. [6–8]). In crux, most of the approximation theoretic ideas in literature master the art of approximation of functions from their equidistant or uniform samples.

Recent studies have raised an interesting question: What is the analog of sampling theory for operators? In simple terms, the key idea is to identify an operator from its response to a probing function or the identifier. In order to formulate the problem, some assumptions are made on the nature of operator. Common examples include smoothness/bandlimited and sparsity priors [9].

Within the framework of bandlimited hypothesis, Pfander discussed "Sampling of Operators" in [10]. This result inherits the non-local flavor that is central to Shannon's sampling theorem—localized reconstruction requires knowledge of all the samples. Krahmer and Pfander then take up the task of localized approximation in [11].

Departing from the bandlimited hypothesis [10], only recently, Heckel and Bölcskei discuss the problem of identification of *Sparse Linear Operators* (SLO) in [12, 13]. This work considers identification of SLO. We begin the discussion with the problem of identifying sparse operators in context of a practical application, that is, mixed-pixel problem in Time-of-Flight (or ToF) imaging.

1.2. Motivation: Mixed-Pixel Problem in ToF Imaging

1.2.1. Time-of-Flight (ToF) Imaging from first principles

Time-of-flight (ToF) imaging is a recent imaging industry development [14] which offers an effective alternative to triangulation and stereo vision based methods for acquiring depth maps. This modality has found a breadth of applications in several areas such as non line-of-sight (NLOS) imaging [15], gesture recognition [16] and computer graphics [17, 18], to name a few. A number of ToF camera manufacturers including Microsoft (Kinect), Mesa, SoftKinetic and PMD provide competitive performance. To an entry level reader, we refer to the book [19] or the survey article [20]. In this area, the **mixed-pixel problem** (MPP) is critical to ToF cameras. There has been a surge of research to solve this problem [19, 21–28]. We introduce the problem starting from first principles.

Extracting Single Depth: For a fixed frequency ω , the ToF camera probes the scene with illuminant $p(t) = DC + \alpha \cos(\omega t)$ —an Amplitude Modulated Continuous Wave (AMCW) where the DC term ensures that optical function $p > 0$. For simplicity, we will ignore the DC term. After reflection and reception from an object at depth d meters from the ToF camera, the probing function becomes,

$$r(t) = \beta \cos(\omega(t - 2d/c)) \equiv \underbrace{\beta \cos(\omega t - \phi_\omega)}_{\text{Reflected Signal}}, \quad (1)$$

where $c = 3 \times 10^8$ m/s is the speed of light and β is the reflection coefficient. The relative delay (or phase $\phi_\omega = \frac{2\omega d}{c}$) with respect to the reference signal encodes the depth information of the scene. Fig. 1. (a) explains the physical setup.

Let $\langle p, r \rangle_I = \int_I p(t) r^*(t) dt$ denote the standard L_2 inner-product between functions $p, r \in L_2$ where $r^*(t)$ is the complex-conjugate of $r(t)$. Following this, cross-correlation between functions p and r is defined as, $C_{p,r}(\tau) = \langle p(t + \tau), r(t) \rangle_{[-\Delta, \Delta]}$. The ToF lock-in pixel [20] then decodes the depth information using the **Four Bucket Principle** which is as follows. Starting with,

$$m(\tau) = \lim_{\Delta \rightarrow \infty} \frac{C_{p,r}(\tau)}{2\Delta} = \frac{1}{2} \alpha \beta \cos(\omega\tau + \phi_\omega), \quad (2)$$

each lock-in pixel computes four discrete measurements, $m[k] = m(k\pi/2\omega)$, $k = 0, \dots, 3$. Let $m_{k,l} = m[k] - m[l]$. The reflection coefficient β and the corresponding phase ϕ are estimated by using, $\tilde{\beta} = (m_{3,1}^2 + m_{0,2}^2)^{1/2} / \alpha$ and $\tilde{\phi} = \arctan(m_{3,1}/m_{0,2})$.

This methodology makes ToF camera a real-time sensing device because the depth estimation is computationally efficient. However, this is a fragile result which only holds for a **strong** assumption. If two or more depths correspond to the same lock-in pixel, the measurements are corrupted. For example, a transparent sheet between the scene and the camera will disrupt the hypothesis much in the same way a photograph gets corrupted during imaging through a reflective surface. Fig. 1. (b) shows an exemplary setting which results in corrupted measurements. Assuming negligible inter-reflections,

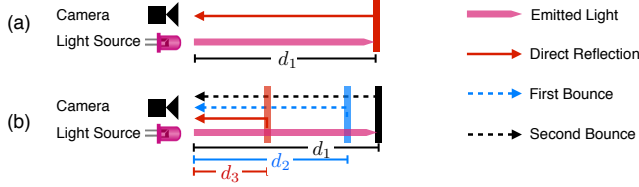


Fig. 1. (a) The ToF camera emits a reference signal. Time delay of arrival from direct reflection encodes the depth d_1 . (b) Demonstration of mixed-pixel problem (MPP): two or more paths contribute to the pixel. The inter-reflections between sheets are assumed to be negligible.

in case of K -depths the reflected function is modeled as, $r(t) = \sum_{k=0}^{K-1} \beta_k \cos(\omega t - \phi_{k,\omega})$ and the measurements take form of,

$$m_K(\tau) \stackrel{(2)}{\underset{\Delta \rightarrow \infty}{\lim}} \frac{c_{p,r}(\tau)}{2\Delta} = \alpha \sum_{k=0}^{K-1} \beta_k \cos(\omega\tau + \phi_{k,\omega}). \quad (3)$$

This is the **mixed-pixel problem (MPP)** in context of ToF imaging as it is impossible to decode the K -depths from $m_K(\tau)$ (cf. Fig. 1 and Fig. 3). This problem has received a lot of attention in the recent past [21–28] due to difficulty of extracting $\phi_{k,\omega} = \frac{2d_k\omega}{c}$ from $m_K(\tau)$. An inspection of (3) reveals an interesting operator identification problem. Let ‘*’ denote convolution operation. Notice that,

$$\sum_{k=0}^{K-1} \beta_k \cos(\omega t - \phi_{k,\omega}) \stackrel{(1)}{=} \cos(\omega t) * \sum_{k=0}^{K-1} \beta_k \delta(t - 2d_k/c).$$

Indeed this problem is associated with a sparse linear operator as,

$$m_K : p \rightarrow p * \underbrace{\sum_{k=0}^{K-1} \beta_k \delta\left(\cdot - \frac{2d_k}{c}\right)}_{\text{Sparse Linear Operator}}, \quad p = \cos(\cdot).$$

However, this is a **special case** that uses AMCW [24] with $p = \cos(\cdot)$. One need not restrict to the class of cosine probing functions.

1.3. Contributions and Organization of this paper

The MPP has been considered in number of papers (cf. [21–28] and references there in). Existing approaches can resolve up to two components and use AMCW/sinusoidal model. There is no mathematical framework that can explain solutions in a general setting. In Section 2.1, we establish a concrete link between mixed pixel problem (MPP) and the sparse linear operator identification (SLO) problem. In Section 2.3, we outline a closed-form solution to recover the SLO without using any sparsity regularized technique. In Section 3.1, we discuss experimental results. We resolve multiple components of mixed-pixels acquired using a ToF camera.

- ▶ **Novelty:** Our approach to identify the sparse linear operator is devoid of any sparsity inducing penalty term. We solve the problem using parameter estimation method for which we derive Cramér-Rao Bounds. The method is easily implementable (cf. Section 3).
- ▶ **Computational Efficiency:** Our solution is closed-form/non-iterative by design. It avoids the computation of regularization parameter which is central to optimization based methods. The complexity of implementation is discussed in Section 2.4.
- ▶ **Practicability:** The approach is verified on practical experiments linked with ToF imaging. We report speed-up over OMP and LASSO as well as lesser mean squared errors (cf. Fig. 2, 3).

2. THE SPARSE OPERATOR IDENTIFICATION PROBLEM

We define the Fourier Transform of p as $\hat{p}(\omega) = F[p] \stackrel{\text{def}}{=} \langle p, e^{j\omega t} \rangle$. Let B_Ω be the set of bandlimited functions, $B_\Omega = \{p : \|p\|_{L_2} < \infty, \hat{p}(\omega) = 0, |\omega| > \Omega\}$. In this paper, we will consider bandlimited probing functions, that is $p \in B_\Omega$.

2.1. Link with the Mixed-Pixel Problem in ToF Imaging

Let $s = p \in B_\Omega$. The link between (5) and the mixed pixel problem can be established by developing $m_K(\tau) \stackrel{(2)}{\underset{\Delta \rightarrow \infty}{\lim}} c_{s,r}(\tau)/2\Delta$ or,

$$\begin{aligned} m_K(\tau) &= \langle p(t + \tau), r(t) \rangle_{t \in \mathbb{R}} \\ &= \int p(t + \tau) \sum_{k=0}^{K-1} \beta_k p\left(t - \frac{2d_k}{c}\right) dt \\ &= \underbrace{C_{p,\bar{p}} * \sum_{k=0}^{K-1} \beta_k \delta(\tau - t_k)}_{2K \text{ Sparse Linear Operator}}, \quad t_k \stackrel{\text{def}}{=} -\frac{2d_k}{c}. \end{aligned} \quad (4)$$

Next, we define the sparse linear operator.

Sparse Linear Operator Let $p \in B_\Omega$, $\bar{p}(t) \stackrel{\text{def}}{=} p(-t)$ and $C_{p,\bar{p}} = (p * \bar{p})$. We define a Sparse Linear Operator of $2K$ parameters as:

$$\mathcal{O}_K[p] : p \rightarrow C_{p,\bar{p}} * \sum_{k=0}^{K-1} \beta_k \delta(\cdot - t_k). \quad (5)$$

Parameters $\{\beta_k, t_k\}_{k=0}^{K-1}$ completely characterize the operator \mathcal{O}_K . From a signals and system perspective, the input/probing function and the output are related as follows:

$$p \rightarrow \boxed{\mathcal{O}_K} \rightarrow \sum_{k \in \mathcal{K}} \beta_k C_{p,\bar{p}}(\cdot - t_k), \quad C_{p,\bar{p}} = (p * \bar{p}).$$

Consequently, we conclude that $m_K(\tau) \stackrel{(4)}{=} \mathcal{O}_K[p](\tau)$.

Inverse Problem: Given $m_K(\tau)$, $\tau \in \mathbb{R}$, how can we characterize the $2K$ -Sparse Linear Operator, or \mathcal{O}_K in (5), with $\{\beta_k, t_k\}_{k=0}^{K-1}$?

2.2. Related Work

In general, (5) is a multi-path/sparse deconvolution problem which has been a topic of several papers starting [29]. Almost all papers use a sparsity inducing penalty term [30, 31]. From a modern perspective, Santosa and Symes [32] introduced the notion of ℓ_2/ℓ_1 -optimization of cost-function to solve the problem (P1),

$$\boxed{\text{P1}} \quad J_\lambda(\mathbf{x}) = \|\mathbf{T}\mathbf{x} - \mathbf{m}\|_{\ell_2}^2 + \lambda \|\mathbf{x}\|_{\ell_1} \quad (6)$$

where \mathbf{T} is a convolution/Toeplitz matrix. The first row/column of \mathbf{T} is the auto-correlation of the probing signal and \mathbf{m} are the measurements. Our problem can be cast as variant of P1 and solved using optimization methods such as Orthogonal Matching Pursuit (OMP) and LASSO [9, 33]. For instance, in [25], we used LASSO and OMP. However, the technique is computationally intensive which is inherent to the sparsity induced optimization recipe. The problem scales with the number of pixels, size of the probing function and the sparsity level. Depth-sensing with compressive sensing methods was used in [34]. Within super-resolution framework, this problem was recently discussed in [35]. The solution is based on optimization.

With the bandlimited hypotheses, our work comes close to the topic of sparse sampling [6–8] with marked differences. The fact that we can design the function p , and hence $C_{p,\bar{p}}(t)$ is a huge degree of freedom which is not the case in sampling theory. In fact, not being able to design p is a restriction in context of sampling theory. All the more, we are *not sampling* a stream of Dirac impulses. We are *interested in system identification*. A similar idea was pursued in [36], however, the solution was based on ℓ_1 penalty term.

2.3. Sparse Linear Operator Identification without Sparse Regularization: Forward Model and Solution to Inverse Problem

Consider a probing function $p \in B_\Omega$ which is T -periodic. In practice, this periodization is a standard trick. It goes by the name of **cyclic prefixing** in OFDM related literature [37]. We use an M-sequence for our practical set up (14). Consequently, p is defined

as,

$$p(t) = \sum_{|m| \leq \Omega} \hat{p}_m e^{jm\omega_0 t}, \quad \omega_0 = 2\pi/T \quad (7)$$

where $\hat{p}_m = \langle p, e^{jm\omega_0 t} \rangle$ are the Fourier series coefficients of $p(t)$. Let $\hat{\phi}_m = \hat{p}_m \hat{p}_m^*$. It is not difficult to show that $\mathcal{C}_{p,\bar{p}}(t) = \phi(t)$,

$$\mathcal{C}_{p,\bar{p}}(t) \stackrel{(7)}{=} \sum_{|m| \leq \Omega} \hat{\phi}_m e^{jm\omega_0 t}. \quad (8)$$

In this setting, we will show that it is possible to reframe problem P1 in (6) as a parameter estimation problem. Observe that the response of the Sparse Linear Operator to the probing function is modeled by,

$$\begin{aligned} \mathcal{O}_K[p](t) &\stackrel{(5)}{=} \mathcal{C}_{p,\bar{p}} * \sum_{k \in K} \beta_k \delta(\cdot - t_k) \\ &= \sum_{k=0}^{K-1} \beta_k \underbrace{\langle \mathcal{C}_{p,\bar{p}}(\tau), \delta(t - \tau - t_k) \rangle}_{\mathcal{C}_{p,\bar{p}}(t-t_k) \equiv \phi(t-t_k)} \\ &\stackrel{(8)}{=} \sum_{|m| \leq \Omega} \hat{\phi}_m \underbrace{\sum_{k=0}^{K-1} \beta_k e^{-j\omega_0 m t_k}}_{b_m(t)} e^{j\omega_0 m t}. \quad (9) \end{aligned}$$

Also, $b_m(t)$ is parameterized by the vector $\mathbf{t} = [t_0, \dots, t_{K-1}]^\top$. On discretization, the above assumes a compact form of,

$$\mathcal{O}_K[p](n) \stackrel{(9)}{=} \mathbf{V}_{\text{IDFT}} \mathbf{D}_{\hat{\phi}} \mathbf{V}_t \boldsymbol{\beta} \stackrel{\text{def}}{=} \mathbf{y}, \quad (10)$$

or simply, $\mathbf{V}_{\text{IDFT}} \mathbf{D}_{\hat{\phi}} \mathbf{b} = \mathbf{y}$ with $n = 0, \dots, N-1$ and where,

- $\boldsymbol{\beta} = [\beta_0, \dots, \beta_{K-1}]^\top, \boldsymbol{\beta} \in \mathbb{R}^{K \times 1}$ is the coefficient vector.
- $\mathbf{V}_t \in \mathbb{C}^{(2\Omega+1) \times (K)}$ is a \mathbf{t} -parameterized Vandermonde matrix with elements, $[\mathbf{V}_t]_{m,k} = \exp(jm\omega_0 t_k), \quad m = -\Omega, \dots, +\Omega$.
- $\mathbf{D}_{\hat{\phi}} \in \mathbb{C}^{(2\Omega+1) \times (2\Omega+1)}$ is the diagonal matrix $\mathbf{D}_{\hat{\phi}} = \text{diag}(\hat{\phi})$, with $\hat{\phi} = [\hat{\phi}_{-\Omega}, \dots, \hat{\phi}_{+\Omega}]^\top \equiv [\hat{p}_{-\Omega} \hat{p}_{-\Omega}^*, \dots, \hat{p}_{\Omega} \hat{p}_{\Omega}^*]^\top$ (8).
- $\mathbf{V}_{\text{IDFT}} \in \mathbb{C}^{(N \times 1) \times (2\Omega+1)}$ is the usual inverse DFT/Vandermonde matrix with matrix elements, $\mathbf{V}_{\text{IDFT}} = [e^{j\omega_0 n m}]_{n,m}$.

We then define $\mathbf{b} = \mathbf{V}_t \boldsymbol{\beta}$. Next, we will outline the solution of the inverse problem of retrieving parameters $\boldsymbol{\beta}$ and \mathbf{t} from \mathbf{y} .

Solving the Inverse Problem: Retrieving $\boldsymbol{\beta}$ and \mathbf{t}

In practice, we have pixel-wise measurements, $m_K(\tau) = \mathcal{O}_K[p](\tau)$ (4). Given p , $\mathbf{D}_{\hat{\phi}}$ is fixed by design. Let the discrete measurement vector be defined as, $\mathbf{y} = \mathbf{m} = [m_K(0), \dots, m_K(N-1)]^\top$ and let \mathbf{A}^+ be the pseudo-inverse of matrix \mathbf{A} . Under the **conditions** that $N \geq 2\Omega + 1$ and $\Omega \geq K$ [38], we have,

$$\mathbf{b} = \mathbf{D}_{1/\hat{\phi}} \mathbf{V}_{\text{IDFT}}^+ \mathbf{y}, \quad \mathbf{b} \in \mathbb{R}^{N \times 1}. \quad (11)$$

Having computed \mathbf{b} , it remains to estimate parameters \mathbf{t} and $\boldsymbol{\beta}$ from,

$$\mathbf{b} = \mathbf{V}_t \boldsymbol{\beta} \Leftrightarrow b_m = \sum_{k=0}^{K-1} \beta_k e^{-j\omega_0 m t_k}. \quad (12)$$

This is the classic line spectrum estimation/Prony's problem [38–42]. Starting with a polynomial, $\mathbf{H}(z), z \in \mathbb{C}$, of form,

$$\mathbf{H}(z) = \sum_{m=0}^{K-1} h_m z^{-m} \equiv \prod_{k=0}^{K-1} (1 - e^{-j\omega_0 t_k} z^{-1}), \quad (13)$$

it is not difficult to show that $h * b = 0 \Leftrightarrow z_k = e^{-j\omega_0 t_k}$, that is, the roots of $\mathbf{H}(z)$ encode the locations $\{e^{-j\omega_0 t_k}\}_{k=0}^{K-1}$ [6,38–42]. Since \mathbf{h} is in the null-space of Toeplitz matrix \mathbf{T} constructed from \mathbf{b} , the singular value decomposition of \mathbf{T} leads to \mathbf{h} which in turn results in $\mathbf{H}(z)$. From the roots of $\mathbf{H}(z)$, that is $z_k = e^{-j\omega_0 t_k}$, we are able to

compute $t_k = -j \arg(z_k) / \omega_0$ and hence \mathbf{V}_t [38]. Given \mathbf{V}_t and \mathbf{b} , we finally compute $\boldsymbol{\beta} = \mathbf{V}_t^+ \mathbf{b}$. This solves the problem.

2.4. Note on Enforcing Sparsity and Computational Complexity

As opposed to ℓ_0 or ℓ_1 penalty based methods, sparsity manifests as a rank-constraint on Hankel/Topelitz matrix used for solving (12). This is an in-built feature of algorithms such as Matrix Pencils [41] or [40], which solve (12). Note that ℓ_0/ℓ_1 based methods start with a dictionary/matrix $[\mathbf{T}]_{m,n} = \mathcal{C}_{p,\bar{p}}(m-n)$ in (6). Hence they are limited in resolution of shifts t_k upto the grid of \mathbf{T} . Our method uses (12). In noiseless setting, it is **not limited** by resolution and t_k 's can be arbitrarily close upto machine precision in simulation. This is a limitation for problem setup in (6). On the other hand, we must remark that (11) must be stabilized in noisy setting. We use Matrix Pencils [41] for the case of noise and [40] for model mismatch.

While the computational complexity of OMP [43] with $\mathbf{T}^{N \times N}$ (6) and for K -sparse signal scales as, $2KN^2 + 2K^2N + 4KN + K^3$, our method uses $(2K+1)2^{\sqrt{2 \log(2K+1)}} \log(2K+1)$ for diagonal matrix multiplication (pointwise multiplication) and $N \log N$ for DFT in (11). What remains is due to Matrix Pencils [41] which is known to be efficient in that none of the terms scale as N^2 .

3. FROM THEORY TO PRACTICE

3.1. Design of Practical Experiments with ToF camera

We demonstrate the efficiency of our method on two practical experiments. To set up the experiment, we first calibrate the probing function to obtain $\mathcal{C}_{p,\bar{p}}$. For this purpose, we use cyclic-prefixing of a code based on M-sequence which is prescribed by,

$$\mathbf{M}_{\text{seq}} = 0101110110001111100110100100001. \quad (14)$$

We omit the details of conversion of \mathbf{M}_{seq} into $p(t)$ and eventually $\mathcal{C}_{p,\bar{p}}(t)$. In Fig. 2. (b), we plot $\mathcal{C}_{p,\bar{p}}(t)$ with its Fourier Series approximation in (—) as well as the Fourier Series coefficients, $\hat{\phi}_m$ in the inset. For this case $\Omega = 29, N = 59$. Each camera pixel measures a mixture of light paths from 3 objects ($K = 3$): a glass unicorn at depth $z = 0$, a plexiglass sheet at depth $z = 2.00$ meters and a wall at depth $z = 3.875$ meters. To resolve the mixed pixels (MPP), we use the SLO formulation in Section 2. Starting with measurements $\mathbf{y} \in \mathbb{R}^{4464 \times 1}$ in Fig. 2. (b), we estimate $\tilde{\boldsymbol{\beta}}$ and $\tilde{\mathbf{t}}$. Unfortunately, it is hard to obtain the ground truth for $\boldsymbol{\beta}$ however, the ground truth for $\mathbf{t} = [2.0139 \ 2.1553 \ 2.2813]^\top$ ps or picoseconds. When we solve the problem using (P1) in (6) using OMP, we obtain $\tilde{\mathbf{t}}_{\text{OMP}} = [2.020 \ 2.156 \ 2.257]^\top$ ps. For our case, we first obtain \mathbf{b} (11) and then use Matrix-Pencils [41] for our problem. Our estimate is reported as $\tilde{\mathbf{t}} = [2.014 \ 2.159 \ 2.2289]^\top$ ps. The estimates are plotted in Fig. 2. (c). We denote the Mean Squared Error or MSE between vectors \mathbf{x} and \mathbf{y} by $\text{MSE}(\mathbf{x}, \mathbf{y})$. Our estimation is better than OMP in MSE sense. For our experiments, $\text{MSE}(\mathbf{t}, \tilde{\mathbf{t}}) = 5.5 \times 10^{-3}$ while, for OMP, $\text{MSE}(\mathbf{t}, \tilde{\mathbf{t}}_{\text{OMP}}) = 4.7 \times 10^{-2}$. Our solution is non-iterative. For the same computing resources on Matlab, our solution offers an average speed-up of 16.7x compared to OMP. This is tested across a patch of $31 \times 31 = 961$ mixed-pixels. The computational time is reported in Fig. 2. (d). In Fig. 2. (a), we compare the result of using Matrix-Pencils [41] and Cadzow's algorithm [40] and plot MSE (in dB) versus Signal-to-Noise Ratio (SNR) for SNR range of -10 to 38 (dB) for different values of oversampling factor η such that $N = 2\eta K + 1$. We consider $\eta = 1, \dots, 5$. Oversampling results in improvement of results. For experiments, we used $K = 3$ with uniformly distributed $\mathbf{t} \in [0, 1]$ and the results are an average over 5000 trials/SNR value. In another experiment, we consider the case of $K = 2, \Omega = 28, N = 57$. A diffusive sheet covers a placard reading: "Time Of Flight," which is 2 meters away. The camera measurements are shown in Fig. 3. (a). Indeed

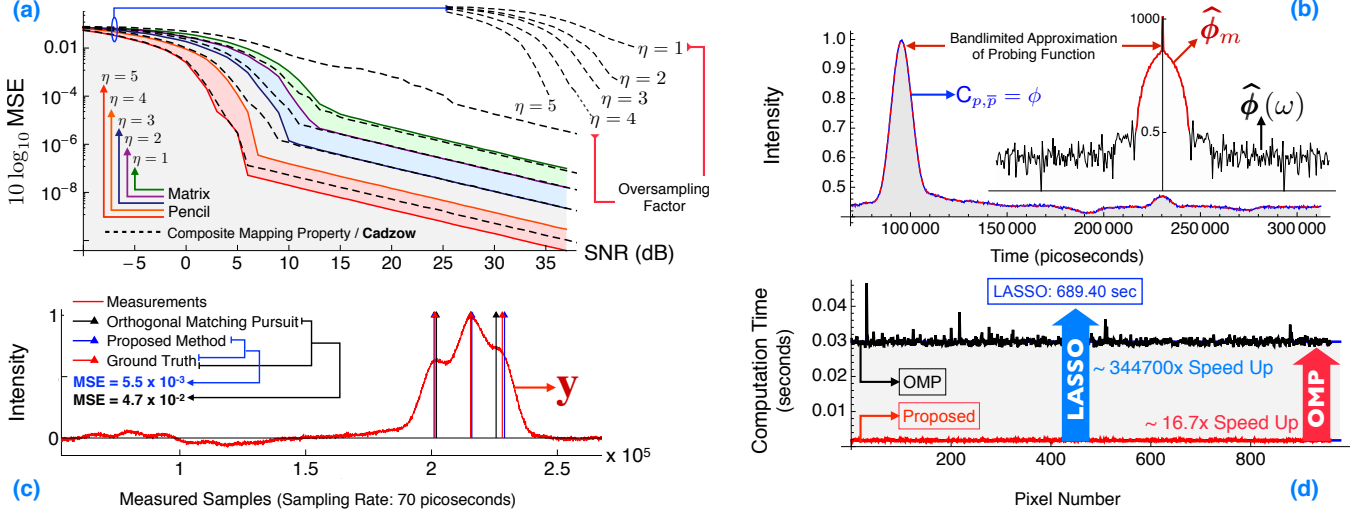


Fig. 2. (a) Performance analysis of methods used for solving $b_m = \sum_{k=0}^{K-1} \beta_k e^{-j\omega_0 m t_k}$ (12) with different oversampling factors $N = 2\eta K + 1$. We compare Matrix Pencil Method [41] with Cadzow’s algorithm [40] for the case of $K = 3$. The parameters are chosen from a uniform distribution. For each SNR value, we average the result over 5000 realizations. (b) Starting with M-sequence in (14) we obtain the calibrated function $C_{p,\bar{p}} = \phi$ in — and its $\Omega = 29$ –term Fourier Series approximation, $\hat{\phi} = B_{\Omega}$ in ---. The inset shows the Fourier Series coefficients (8). (c) Mixed–Pixel Problem for $K = 3$ mixing paths. The measurements \mathbf{y} are marked in —. Ground truth and estimates using OMP in (6) and our method are also marked. (d) We report the computation time involved with using LASSO, OMP and our non–iterative method. OMP requires ~ 0.03 seconds per pixel while our method (using Matrix Pencils) requires ~ 0.002 seconds. This result is consistent over a set of 961 pixels. LASSO is computationally intensive. For one pixel, the requirement is 689.40 seconds.

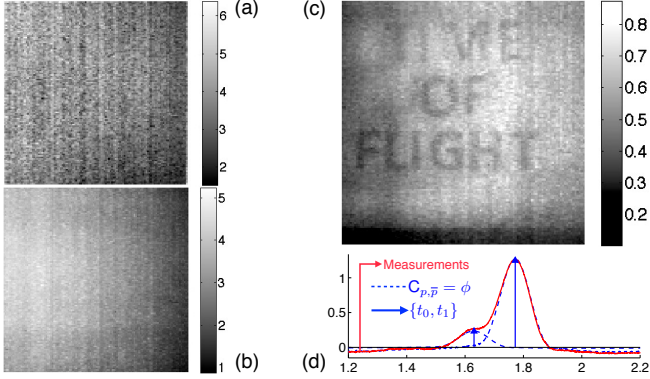


Fig. 3. (a) Measurements (—) of a scene where a translucent/diffusing sheet $\{\beta_0, t_0\}$ hides a placard $\{\beta_1, t_1\}$. The mixed–pixels correspond to the case of $K = 2$. Using our method, the mixed–pixels in (a) are decomposed into the diffusing sheet in (b) and the placard that reads, “Time of Flight” in (c). (d) We show measurements \mathbf{y} for one of the pixel of 120×120 image. These measurements are decomposed into shifted and amplitude scaled versions of $C_{p,\bar{p}} = \phi$ marked in - - - -. Depths $\propto \{t_0, t_1\}$ are marked with \rightarrow .

it is impossible to read anything. However, since each measurement corresponds to a mixed–pixel, we can use the sparse operator identification method to decouple the measurements. Consequently, in Fig. 3. (b), we show the strong reflection from the translucent sheet, that is $\{\beta_0, t_0\}$. Since we have estimated $\{\beta_1, t_1\}$, it is possible to read through the translucent/diffusive sheet as shown in Fig. 3. (c). In Fig. 3. (d), we show the measurements \mathbf{y} and estimates $\hat{\beta}, \hat{t}$.

3.2. Cramér–Rao Lower Bounds (CRB)

With zero–mean, Gaussian noise assumption on e_n and covariance matrix $\Sigma = \mathcal{E}[\mathbf{e}\mathbf{e}^T] = \sigma^2 \mathbf{I}$ we model N noisy measurements (10) as, $y_n = \mathcal{O}_K[p](n) + e_n \Leftrightarrow \mathbf{y} = \mathbf{m} + \mathbf{e}$. The parameter vector of interest is $\tilde{\boldsymbol{\theta}} = [\tilde{t}_0, \dots, \tilde{t}_{K-1}, \tilde{\beta}_0, \dots, \tilde{\beta}_{K-1}]^T$. Within this frame–

work, the CRB of an unbiased estimator of the parameter vector $\boldsymbol{\theta}$ holds such that, $\mathcal{V}(\hat{\boldsymbol{\theta}}) \leq \mathbf{J}^{-1}(\boldsymbol{\theta})$ where \mathbf{J} is the Fisher Information Matrix and \mathcal{V} is the variance operator. Following the CRB simplification for Gaussian distribution (cf. Appendix 3C [44]), we have, $\mathbf{J}(\boldsymbol{\theta}) = \sigma^{-2} \boldsymbol{\Upsilon}^T \boldsymbol{\Upsilon}$. For simplicity we consider $K = 1$, then,

$$\boldsymbol{\Upsilon}^T = \begin{bmatrix} -\beta_0 \phi'(1-t_0) & \dots & \beta_0 \phi'(N-t_0) \\ \phi(1-t_0) & \dots & \phi(N-t_0) \end{bmatrix}.$$

Since the anti–diagonal of $\mathbf{J}(\boldsymbol{\theta})$ is zero, the variance $\mathcal{V}(\tilde{\boldsymbol{\theta}}) \geq \sigma^2 \text{diag}(\beta_0^2 N \omega_0^2 S_m, N S_1)$ with $S_m = \sum_m m^2 \hat{\phi}_m^2$. Set $\text{SNR} = \sigma^2 / \beta_0^2$, we obtain the spread in estimation of t_0 and β_0 as follows:

$$\frac{\Delta t_0}{T} \geq \frac{1}{2\pi \sqrt{S_m N} \cdot \text{SNR}} \quad \text{and} \quad \frac{\Delta \beta_0}{|\beta|} \geq \frac{1}{\sqrt{S_1 N} \cdot \text{SNR}}.$$

4. CONCLUSIONS

As a follow–up on the recent investigations regarding identification of operators from its response to a probing function [10–13], we discuss a non–iterative method for the problem of sparse linear operator identification [13]. Our method is devoid of any sparsity inducing penalty term. Our work finds application in context of resolving mixed pixels in Time–of–Flight imaging for which our theoretical set corroborates with practical experiments. We report a speed up in computation time over previously used methods. Our method leads to lesser mean squared error.

5. ACKNOWLEDGEMENTS

AB thanks Prof. Thierry Blu for a number of detailed discussions. This work has benefited from his advise during AB’s stay at CUHK in 2009–10. Prof. Felix Kraher’s wonderful introduction to the topic of Sampling Operators at BASP meeting in 2013 is duly acknowledged. Prof. Laurent Daudet’s remarks on the first version of this paper have been very useful. Refael Whyte’s help with experiments has been instrumental in making our theory practicable. AK was supported by a Charles Stark Draper Fellowship.

6. REFERENCES

- [1] A. J. Jerri, "The Shannon sampling theorem—its various extensions and applications: A tutorial review," *Proc. IEEE*, vol. 65, no. 11, pp. 1565–1596, Nov. 1977.
- [2] C. D. Boor, R. A. Devore, and A. Ron, "Approximation from shift-invariant subspaces of $L_2(\mathbb{R}^d)$," *Trans. Amer. Math. Soc.*, vol. 341, no. 2, pp. 787–806, 1994.
- [3] M. Unser, "Sampling—50 years after Shannon," *Proc. IEEE*, vol. 88, no. 4, pp. 569–587, 2000.
- [4] Y. M. Lu and M. N. Do, "A theory for sampling signals from a union of subspaces," *IEEE Trans. Signal Proc.*, vol. 56, no. 6, pp. 2334–2345, 2008.
- [5] A. Bhandari and A. I. Zayed, "Shift-invariant and sampling spaces associated with the fractional Fourier domain," *IEEE Trans. Signal Proc.*, vol. 60, no. 4, pp. 1627–1637, 2012.
- [6] T. Blu, P.-L. Dragotti, M. Vetterli, P. Marziliano, and L. Coulot, "Sparse sampling of signal innovations," *IEEE Signal Proc. Mag.*, vol. 25, no. 2, pp. 31–40, March 2008.
- [7] M. Vetterli, P. Marziliano, and T. Blu, "Sampling signals with finite rate of innovation," *IEEE Trans. Signal Proc.*, vol. 50, no. 6, pp. 1417–1428, 2002.
- [8] A. Bhandari and P. Marziliano, "Sampling and reconstruction of sparse signals in fractional Fourier domain," *IEEE Signal Proc. Letters*, vol. 17, no. 3, pp. 221–224, 2010.
- [9] M. Elad, *Sparse and redundant representations: from theory to applications in signal and image processing*, Springer, 2010.
- [10] G. Pfander, "Sampling of operators," *Journal of Fourier Analysis and Applications*, pp. 1–39, 2013.
- [11] F. Krahmer and G. Pfander, "Local sampling and approximation of operators with bandlimited Kohn–Nirenberg symbols," *arXiv*, , no. 1211.6048, 2013.
- [12] R. Heckel and H. Bölcskei, "Compressive identification of linear operators," in *Proc. of IEEE Intl. Sym. on Info. Theory (ISIT)*, Aug. 2011, pp. 1412–1416.
- [13] R. Heckel and H. Bölcskei, "Identification of sparse linear operators," *IEEE Trans. Info. Theory*, 2013.
- [14] P. Lange, R. and Seitz, "Solid-state time-of-flight range camera," *IEEE J. of Quantum Elec.*, vol. 37, no. 3, pp. 390–397, 2001.
- [15] A. Velten, T. Willwacher, O. Gupta, A. Veeraraghavan, M. Bawendi, and R. Raskar, "Recovering three-dimensional shape around a corner using ultrafast time-of-flight imaging," *Nature Communications*, vol. 3, pp. 745, 2012.
- [16] P. Breuer, C. Eckes, and S. Müller, "Hand gesture recognition with a novel IR time-of-flight range camera—a pilot study," in *Comp. Vis./Comp. Graphics Collab. Tech.*, pp. 247–260. Springer, 2007.
- [17] A. Kolb, E. Barth, R. Koch, and R. Larsen, "Time-of-Flight sensors in computer graphics," in *Proc. Eurographics*, 2009, pp. 119–134.
- [18] A. Kadambi, A. Bhandari, R. Whyte, A. Dorrington, and R. Raskar, "Multiplexing illumination via low cost sensing and nanosecond coding," in *IEEE International Conference on Computational Photography (ICCP)*, March 02-04 2014.
- [19] M. Hansard, S. Lee, O. Choi, and R. Horaud, *Time-of-flight cameras: principles, methods and applications*, Springer, 2013.
- [20] S. Foix, G. Alenya, and C. Torras, "Lock-in time-of-flight (tof) cameras: a survey," *IEEE Sensors Journal*, vol. 11, no. 9, pp. 1917–1926, 2011.
- [21] D. Jiménez, D. Pizarro, M. Mazo, and S. Palazuelos, "Modelling and correction of multipath interference in time of flight cameras," in *Comp. Vis. and Patt. Rec. (CVPR)*, 2012, pp. 893–900.
- [22] M. Frank, M. Plaue, H. Rapp, U. Köthe, B. Jähne, and F. A. Hamprecht, "Theoretical and experimental error analysis of continuous-wave Time-of-Flight range cameras," *Proc. SPIE Conf. on Vis. Commun. and Image Proc.*, vol. 48, no. 1, pp. 013602—013602, 2009.
- [23] S. Fuchs, "Multipath interference compensation in time-of-flight camera images," in *Intl. Conf. Patt. Rec. (ICPR)*, 2010, pp. 3583–3586.
- [24] A. Bhandari, A. Kadambi, R. Whyte, C. Barsi, M. Feigin, A. Dorrington, and R. Raskar, "Resolving multipath interference in time-of-flight imaging via modulation frequency diversity and sparse regularization," *Optics Letters*, vol. 39, no. 7, 2014.
- [25] A. Kadambi, R. Whyte, A. Bhandari, L. Streeter, C. Barsi, A. Dorrington, and R. Raskar, "Coded time of flight cameras: Sparse deconvolution to address multipath interference and recover time profiles," in *SIGGRAPH Asia 2013 (to appear)*.
- [26] J. P. Godbaz, A. A. Dorrington, and M. J. Cree, "Understanding and ameliorating mixed pixels and multipath interference in amcw lidar," in *TOF Range-Imaging Cameras*, pp. 91–116. Springer, 2013.
- [27] A. P. Jongenelen, D. G. Bailey, A. D. Payne, A. A. Dorrington, and D. A. Carnegie, "Analysis of errors in tof range imaging with dual-frequency modulation," *IEEE Trans. on Inst. and Measurement*, vol. 60, no. 5, pp. 1861–1868, 2011.
- [28] D. Droschel, D. Holz, and S. Behnke, "Multi-frequency phase unwrapping for time-of-flight cameras," in *IEEE/RSJ Intl. Conf. on Intell. Robots and Systems*, 2010, pp. 1463–1469.
- [29] J. F. Claerbout and Muir, F., "Robust modelling with erratic data," *Geophysics*, vol. 38, no. 1, pp. 826–844, 1973.
- [30] H. L. Taylor, S. C. Banks, and J. F. McCoy, "Deconvolution with the ℓ_1 norm," *Geophysics*, vol. 44, no. 1, pp. 39–52, 1979.
- [31] J. J. Fuchs, "Multipath time-delay detection and estimation," *IEEE Trans. Signal Proc.*, vol. 47, no. 1, pp. 237–243, 1999.
- [32] F. Santosa and W. W. Symes, "Linear inversion of band-limited reflection seismograms," *SIAM J. on Sci. and Stat. Comp.*, vol. 7, no. 4, pp. 1307–1330, 1986.
- [33] "Special issue on compressed sensing," *IEEE Signal Processing Magazine*, vol. 25, no. 2, 2008.
- [34] P. T. Boufounos, "Depth sensing using active coherent illumination," in *Proc. IEEE Int. Conf. Acoustics, Speech, and Signal Processing*, March 25-30 2012.
- [35] E. J. Candès and C. Fernandez-Granda, "Towards a mathematical theory of super-resolution," *Commun. on Pure and Appl. Math.*, 2013.
- [36] S. Levy and P. K. Fullagar, "Reconstruction of a sparse spike train from a portion of its spectrum and application to high-resolution deconvolution," *Geophysics*, vol. 46, no. 9, pp. 1235–1243, 1981.
- [37] B. Muquet, Z. Wang, G. B. Giannakis, M. De Courville, and P. Duhamel, "Cyclic prefixing or zero padding for wireless multicarrier transmissions?," *IEEE Trans. Commun.*, vol. 50, no. 12, pp. 2136–2148, 2002.
- [38] G. Plonka and M. Wischerhoff, "How many Fourier samples are needed for real function reconstruction?," *Jour. of Appl. Math. and Comp.*, vol. 42, no. 1-2, pp. 117–137, 2012.
- [39] P. Stoica and R.L. Moses, *Introduction to spectral analysis*, vol. 89, Prentice Hall Upper Saddle River, NJ, 1997.
- [40] J. Cadzow, "Signal enhancement—A composite property mapping algorithm," *IEEE Trans. Signal Proc.*, vol. 36, no. 1, pp. 49–62, 1988.
- [41] Y. Hua and T. K. Sarkar, "Matrix pencil method for estimating parameters of exponentially damped/undamped sinusoids in noise," *IEEE Trans. Signal Proc.*, vol. 38, no. 5, pp. 814–824, 1990.
- [42] "Special issue on spectral estimation," *Proc. IEEE*, vol. 70, Sept. 1982.
- [43] R. Rubinstein, M. Zibulevsky, and M. Elad, "Efficient implementation of the K-SVD algorithm using batch orthogonal matching pursuit," *CS Technion*, 2008.
- [44] S. Kay, *Fundamentals of Statistical Signal Processing: Estimation Theory*, Prentice-Hall, 1993.